Mechanical Resistance in Decapod Claw Denticles: Contribution of Structure and Composition

Miranda N. Rosen[1], Kerstin A. Baran[1], Justin N. Sison[1], Brittan V. Steffel[2], W. Christopher Long[3], Robert J. Foy[3], Kathryn E. Smith[4], Richard B. Aronson[2], Gary H. Dickinson[1*]

[1]Department of Biology, The College of New Jersey, Ewing, NJ 08628, USA

[2]Department of Ocean Engineering and Marine Sciences, Florida Institute of Technology, Melbourne, FL 32901, USA

[3]NOAA, National Marine Fisheries Service, Alaska Fisheries Science Center, Resource Assessment and Conservation Engineering Division, Kodiak Laboratory, 301 Research Ct., Kodiak, AK 99615, USA

[4]The Marine Biological Association, The Laboratory, Citadel Hill, Plymouth, PL1 2PB, UK

*Corresponding author: Gary H. Dickinson, dickinga@tcnj.edu

Keywords: calcification, microhardness, cuticle, biomineralization, chitin, calcite, crustacean

Abstract

The decapod crustacean exoskeleton is a multi-layered structure composed of chitin-protein fibers embedded with calcium salts. Decapod claws display tooth-like denticles, which come into direct contact with predators and prey. They are subjected to more regular and intense mechanical stress than other parts of the exoskeleton and therefore must be especially resistant to wear and abrasion. Here, we characterized denticle properties in five decapod species. Dactyls from three brachyuran crabs (*Cancer borealis, Callinectes sapidus,* and *Chionoecetes opilio*) and two anomuran crabs (*Paralomis birsteini* and *Paralithodes camtschaticus*) were sectioned normal to the contact surface of the denticle, revealing the interior of the denticle and the bulk endocuticle in which it is embedded. Microhardness, micro- and ultrastructure, and elemental composition were assessed along a transect running the width of the cuticle using microindentation hardness testing, optical and electron microscopy (SEM), and energy dispersive X-ray spectroscopy (EDS), respectively. In all species tested, hardness was dramatically higher—up to ten times—in the denticle than in the bulk endocuticle. Likewise, in all species there was an increase in packing density of mineralized chitin-protein fibers, a decrease in width of the pore canals that run through the cuticle, and a decrease in phosphorous content from endocuticle to denticle. The changes in hardness across the cuticle, and the relationship between hardness, calcium, and magnesium content, however, varied among species. Although mechanical resistance of the denticles was exceptionally high in all species, the basis for resistance appears to differ among species.

1. Introduction

The exoskeleton of crustaceans provides support to the body and acts as armor, protecting the animals from predatory attacks as well as environmental threats such as desiccation [1-3]. In decapod crustaceans, the exoskeleton consists of multiple layers, that all contribute to the overall structure of the cuticle. The thinnest, outermost layer, known as the epicuticle, lacks chitin; it is composed primarily of waxes and contains discontinuous clusters of calcium salts [4-6]. The exocuticle, which underlies the epicuticle, contains stacked layers of chitin-protein fibers that vary regularly in orientation (i.e. twisted plywood or Bouligand structures) [4, 7]. The endocuticle is similar in structure to the exocuticle, but the density of chitin-protein layers is lower than in the exocuticle [2]. The exo- and endocuticle layers are embedded with amorphous calcium carbonate or nanocrystalline calcite, which in crabs form mineral tubes around the chitin-protein fibers [4, 8, 9]. Variations in both mineral content and stacking density of chitin-protein fibers can contribute to differences in mechanical strength of the cuticle among regions and species [2, 7, 9]. Pore canals cross through the endo- and exocuticle, exhibiting a helical or twisted ribbon morphology [4]. These structures also contribute to the mechanical properties of the cuticle; their ductility likely increases plasticity of the cuticle [6, 7, 10].

Although calcium carbonate is typically the principal material for reinforcing the exoskeleton in crustaceans, calcium phosphate is also used [6, 11, 12]. For example, an outer calcium phosphate layer was identified in the mandible teeth of various crustaceans [11, 13]. Analogous to vertebrate enamel, incorporation of calcium phosphate results in a very hard outer layer that serves as reinforcement for mechanically challenged sites and can also provide chemical resistance [11].

Decapod crustaceans, including those belonging to the infraorders Brachyura and Anomura, have two claws (chelae) located at the anterior of their bodies, which are used to capture prey, to defend against predators, and in mating. Because the claws are heavily used for feeding and defense, their mechanical properties are enhanced as compared to the carapace and legs [2, 7, 9, 14, 15], and claws typically have an increased level of calcification [7, 9, 15, 16]. Constant use of the claws causes them to wear, and in some cases break. Wear and damage reduce the feeding efficiency and fighting ability of crabs, therefore reducing their reproductive success and overall fitness [17, 18].

The claw of a decapod crustacean is composed of two articulating portions: the upper (dorsal) portion, the dactyl, is movable (often referred to as a "movable finger") and the lower (ventral) portion, the pollex, is fixed (the "fixed finger"). In some crab species, the inner portions of both the dactyl and pollex display tooth-like denticles. Structural analyses have shown that these denticles are composed primarily of modified endocuticle, with little or no epi- or exocuticle present in this region in adult crabs [16]. The denticles serve as the points of contact in the capture of prey and defense against predators; it would therefore be expected for the denticles to be abrasion-resistant and have mechanical properties superior to those of the rest of the claw. Indeed, Waugh et al. [16] found that microhardness of the denticles was ~2.5 times greater than the bulk claw endocuticle in the brachyuran *Scylla serrata,* and in *Callinectes sapidus* denticles were about four times greater than the bulk endocuticle.

Despite the broad importance of the claw denticles in feeding and defense and their impressive mechanical resistance, comprehensive assessments of these structures are limited. Here, we sought to characterize the mechanical properties of the denticles in a range of decapod species, and to assess the basis for their mechanical resistance. Given the strong evolutionary pressure on feeding and defensive structures [17, 18], we hypothesized that the occurrence of enhanced denticle mechanical properties is widespread among decapod crab species. To assess this hypothesis, a taxonomically and geographically diverse group of five benthic durophagous crab species were tested. These included three brachyuran crabs (*Cancer borealis, Callinectes sapidus,* and *Chionoecetes opilio*) and two anomuran crabs (*Paralomis birsteini* and *Paralithodes camtschaticus*). Brachyurans are considered "true crabs" whereas anomurans belong to an infraorder that includes hermit crabs and evolved the crab-like body form independently [19, 20]. In all species, we quantified microhardness, micro- and ultrastructure, and elemental composition along a transect running the width of the cuticle from the bulk endocuticle through the denticle.

2. Materials and methods

2.1. Specimen collection

King crabs (*Paralomis birsteini*) were captured in February 2015 off the continental slope of Marguerite Bay, western Antarctic Peninsula at a depth of approximately 1350 m [21]. Jonah crabs (*Cancer borealis*) captured in the Gulf of Maine at a depth of approximately 50 m were purchased from D.C. Air and Seafood Outlet in Winter Harbor, Maine in July of 2016. Blue crabs (*Callinectes sapidus*) were trapped at depths of 30 m or less in Florida, USA, and purchased at Direct Seafood Outlet located in Melbourne, Florida. Snow crabs (*Chionoecetes*

opilio) were collected by members of NOAA's Kodiak Laboratory from different sites along the Bering Sea during the eastern Bering Sea trawl survey [22]. Red king crabs (*Paralithodes camtschaticus*) were collected in pots in Bristol Bay, Alaska, during commercial fishing and were held in tanks in ambient seawater at the Kodiak Laboratory for approximately two years before use. All samples were stored at -20°C prior to analysis. Samples were transported from the Florida Institute of Technology or NOAA's Kodiak Laboratory to The College of New Jersey for analysis.

2.2. Transect preparation

For the analyses described here, a total of three replicate dactylus samples per species were used, with the exception of *P. camtschaticus* for which only two crabs were available. In all cases, the dactylus (movable finger) was taken from the right (major) chela. The dactyli were cut from the chela using a high-speed diamond band saw (Gryphon), and samples were cut to fit within the dimensions of 3.175-cm-diameter, two-part mounting cups used during the embedding process described below. The anterior tips of *C. opilio* dactyli were cut off to access the dactyl cavity. Any visible tissue was extracted from inside the cavity of the dactylus using forceps. Samples were placed on a lyophilizer (Labconco 12 Port Dry Ice Benchtop or Yamato DC41-A) for approximately 18 hours to remove any moisture that may inhibit the embedding process. Prior to embedding, each dactylus sample was secured to the bottom of a mounting cup using cyanoacrylate glue (Loctite® Control Gel) at an angle that would expose a cross section through the midline of the denticles during grinding/polishing. To ensure that all voids were filled, the cavity of each dactylus sample was first filled with epoxy (Allied High Tech EpoxySet) using a pipettor. Embedding cups were then filled with epoxy and samples were left to cure at room

temperature for approximately 24 hours. For *C. opilio* and *P. camtschaticus*, samples were placed under vacuum at ~75 kPa for 5 minutes immediately after addition of epoxy to further ensure penetration of epoxy into sample voids.

After embedding, all samples were polished using a grinder polisher machine to reach the midline through the dactyl and to ensure a smooth, flat sample surface for microhardness testing. *P. birsteini* and *C. borealis* first were cut down the midline using a low-speed diamond saw (Allied High Tech Products) prior to polishing [15]. *P. birsteini and C. borealis* and were ground and polished on a manual grinder polisher machine (Allied High Tech M PREP-5), whereas *C. sapidus*, *C. opilio*, and *P. camtschaticus* were ground and polished on an automated grinding/polishing system (Allied High Tech METPREP 3 PH-4). The backside of each sample was ground using a 180 grit silicon carbide paper for the manual polisher and a 120 grit silicon carbide paper for the automated polisher. Aside from this first step, all other steps were the same for both the manual and automated polishers. Samples were ground through a series of silicon carbide papers (320, 600, and 800 grit), followed by polishing with a 1 μm polycrystalline diamond and a 0.04 μm colloidal silica suspension. Between each polishing step, samples were cleaned with a 2% solution of Micro Organic Soap. All polishing products were purchased from Allied High Tech Products, Inc. Samples were dried using compressed air and placed in a desiccator for at least 24 hours before testing.

2.3. Microhardness

Vickers microhardness testing was conducted using a hardness testing machine (Mitutoyo HM-200). Samples were tested when dry. Although testing of fully hydrated samples was not possible

due to the need to dry samples before embedding, testing of dactyl endocuticle samples when dry and again when rehydrated showed no effect of hydration on dactyl endocuticle hardness (Dickinson et al., *unpublished results*). Indents were made at a 10 g load, 5 sec dwelling time, along a transect starting in the denticle region and running through the length of the endocuticle (Figs. 1–5). The first indent made in the denticle was placed at least 30 µm away from the edge of the sample and successive indents were made every 100 µm until the end of the endocuticle was reached. The number of indents made per sample was dependent on the thickness of the sample and varied from 8 in *C. opilio* to 40 in *C. borealis*. Digital images were taken immediately after each indentation using a Zeiss Axiocam 305 color camera. Indent diagonals were measured using digital images and microhardness values were calculated using the equation $HV = 1.854*F/d^2$, where F is the force in kg and d^2 is the mean diagonal length in mm.

2.4. Ultrastructure, pore canal width, and elemental composition

A scanning electron microscope (SEM) was used to image five regions of each sample along the same transect where microhardness measurements were taken. Representative images showing these regions are presented in Figs. 1–5, labelled as A–E. Region C was centered at the visible transition from bulk endocuticle to denticle. Regions A and B were within in the bulk endocuticle, with region A as close to the inner edge of the sample as possible while avoiding edge effects (typically ~10% of the endocuticle distance away from the edge) and region B located approximately halfway between the inner edge and the transition. Regions D and E were in the denticle and followed the same pattern as described for the endocuticle, with region E as close to the outer edge of the sample as possible (while avoiding edge effects) and region D located approximately halfway between the outer edge and the transition. Note that the denticles

are a modified portion of the endocuticle layer of the exoskeleton [16]. For simplicity, we refer to the bulk endocuticle, which runs along the entirety of the dactylus, as “endocuticle”, and the modified portion of the endocuticle that composes the denticles as “denticle”. In each case, images were taken just anterior to the indents, to avoid inclusion of the indent itself in the image. Images were taken at 5000 X, 15kV accelerating voltage, at 50 Pa on a field emission SEM (Hitachi America, SU5000). A working distance of approximately 8 mm was used for all samples.

In order to quantitatively assess structural change within the cuticle, the width of pore canals in a subset of visible canals was measured on SEM images using image analysis software (Image J v. 1.52 [23]). Six pore canals were randomly selected for quantification in each image. For selection, a 2 μm^2 grid was first placed on the image. Pairs of random numbers were generated using a random number generator, and each pair was used as coordinates to identify specific canals for analysis. Canal width was measured using the linear measurement tool along the short axis of the canal. The measured width axis was perpendicular to, and midway along, the longest axis of the canal.

The same areas used for SEM imaging were also used for elemental analysis. An energy dispersive X-ray spectroscopy (EDS) detector (AMTEK Materials Analysis Division, Octane Plus) was used to determine elemental composition at each of the five areas in all samples. Imaging conditions typically resulted in a count rate of 5,000–10,000 counts per second, and an amp time of 3.84 was applied.

2.5. Microstructure

To enable direct comparison of microhardness, ultrastructure, and composition along each transect, composite images of each sample were taken after microhardness testing. Images were taken using a Zeiss Axioscope.A1 reflected light microscope with a Zeiss Axiocam 105 color camera. The distance between each indent along the transect, total endocuticle length, and denticle length were measured using Zeiss Zen 2.3 software. The distance between SEM imaging regions (A–E) was also measured.

2.6. Statistical Analyses

Multivariate statistics were used to explore the differences among species and regions (A–E) in mineral content, microhardness, and pore canal width (Primer, v. 6.1.15, Primer-E). For microhardness, the indent closest to each of the imaged regions (A–E) was selected and these data were used in analyses. Measurements were normalized (expressed in terms of their z-scores) prior to analysis. Principal component analysis (PCA) was performed and principal components (PCs) explaining more than 10% of the variance in the data were retained. A crossed two-way analysis of similarity (ANOSIM) was performed on a Euclidian-distance similarity matrix to test for difference among species and regions. Given the differences observed (see results text) Spearman rank correlation analyses were performed to further assess factors within species that contribute to mechanical properties across the cuticle (SPSS, v. 23, IBM Analytics). Specifically, the relationships between microhardness and calcium content, magnesium content, and pore canal width were assessed for each crab species. To account for potential type I error associated with conducting multiple correlations analysis, a Benjamini-Hochberg procedure at a false discovery rate of 0.1 was applied to determine statistical significance.

3. Results

3.1. Microhardness

Microhardness increased dramatically from endocuticle to denticle in all species tested. *P. birsteini* showed the largest increase in microhardness from region A to E, showing over a ten-fold difference in hardness between the two regions (Table 1). The increase in hardness from bulk endocuticle to denticle tended to be smallest in *C. sapidus*, but even in this species, the denticles were nearly four times harder than the bulk endocuticle. The gradient of hardness across the cuticle, however, varied among species. In *C. sapidus*, *P. birsteini, C. opilio,* and *P. camtschaticus* hardness was low in the bulk endocuticle (typically between 20 and 75 VHN) and exhibited a sharp increase in hardness (typically to 200–300 VHN) at or near the visual transition to the denticle (Figs. 1, 3–5). The increase in hardness across the cuticle was much more gradual in *C. borealis* (Fig. 2). In this species, bulk endocuticle hardness tended to be higher (~50–150 VHN) with only a modest and gradual increase at the visual transition to the denticle.

3.2. Elemental composition

Calcium content increased from region A in the endocuticle to region E in the denticle in all crab species tested (Table 1). The change in calcium content from region A to region E tended to be greatest in *C. sapidus* and *C. opilio*, at 25 and 26%, respectively. Patterns with respect to magnesium content varied among species; *C. sapidus* showed a slight increase in magnesium content from region A to E, whereas all other species showed a reduction in magnesium in the denticle (by as much as 68% in *C. opilio*) (Table 1). Phosphorus was only present in the endocuticle and transition region; it was never identified in the denticle (Table 1).

3.3. Multivariate and correlation analyses

In PCA of the mechanical, elemental, and structural variables the first three PCs were retained, with the first two explaining more than 72% of the variance in the data (Table 2). The first PC was positively associated with calcium and hardness and negatively associated with phosphorous and magnesium (Table 2, Fig. 6). Within each species, the observations made in different regions fell along a gradient of PC1 scores, with observations in the endocuticle having low PC1 scores and observations in the denticle having high scores. The second PC had a strong negative correlation with pore canal width and a positive correlation with magnesium and calcium (Table 2, Fig. 6). Within different regions, observations made on different species fell along a gradient of PC2 scores. The third PC had low explanatory power and did not have a clear interpretation. ANOSIM indicated that the mechanical, elemental, and structural variables differed among both areas (Global $R = 0.727$, $p = 0.000001$) and species (Global $R = 0.746$, $p = 0.000001$). Pairwise comparisons indicated that all species differed from all other species ($p < 0.0004$ in all cases except for *P. birsteini* vs. *P. camtschaticus* where $p = 0.031$). All areas also differed from all other areas ($p < 0.011$ in all cases; Table S1) except that areas A and B did not differ from each other ($p = 0.055$).

In *C. sapidus*, *C. borealis*, *C. opilio*, and *P. camtschaticus* correlation analyses revealed a significant positive relationship between calcium content and microhardness (Table 3), implying that the cuticle was harder in regions with a higher calcium content. In two of these species (*C. borealis* and *C. opilio*), a significant negative relationship was also found between microhardness and magnesium content (i.e., microhardness was higher in regions where magnesium content

was lower). For *P. birsteini*, neither calcium nor magnesium content was significantly correlated with microhardness. For all five species, a significant negative relationship was found between microhardness and pore canal width, implying that the cuticle was harder in regions with lower pore canal width.

3.4. Micro- and ultrastructure

Light microscopy imaging of dactyl samples showed clear twisted plywood structures (laminations), appearing as alternating light and dark regions, within the bulk endocuticle of all species (Figs. 1–5; Fig. S1). These laminations continued through the transition zone into the proximal portion of the denticle. Moving distally within the denticles, twisted plywood structures became difficult to discern by light microscopy in all species except *C. sapidus*. In *C. sapidus*, Twisted plywood structures were visible at the periphery of the denticles, but were not observed within the central-most portion. Of the five species tested, *P. camtschaticus* was the only one to consistently show a small amount of exocuticle (~100 µm thick) covering the denticle (Fig. 5; Fig. S1). The exocuticle in *P. camtschaticus* extended along the entire length of the dactylus, covering the denticles and extending through the groves between denticles. In the other species tested, the exocuticle was lacking on the denticles; exocuticle was present in the regions of the dactylus proximal to the denticles, and within the groves between denticles, but ended abruptly where the denticles emerged (Fig. S1).

SEM imaging revealed a distinct shift in structure from the bulk endocuticle to the denticle in all species tested. In the back-scattered electron images provided in Figs. 1–5, image brightness corresponds to sample density (specifically Z-contrast). Hence bright areas within the images are

high density (high Z-contrast) and dark areas are low density (low Z-contrast). In all five species, there is a clear increase in sample density moving from the bulk endocuticle to the denticle. Structural features of note include pore canals (marked "PC") and mineralized chitin-protein fibers (marked "CF"). Chitin-protein fibers are encased by mineral tubes [6]. Within the regions marked "CF", the chitin-protein fraction shows as dark striations (low Z-contrast) alternating with brighter striations of surrounding mineral (high Z-contrast).

Overall structure, and the changes in structure across the cuticle, were similar in all species. The width of pore canals that were visible in the sectioned plane decreased from endocuticle to denticle (Table 1). The change in pore canal width from region A to E tended to be highest for *C. borealis* and lowest for *C. sapidus* (Figs. 1–5). Within the denticle, the highest density regions were typically found at the periphery of the pore canals. This is particularly evident for *C. sapidus* and *C. borealis* (i.e. Fig. 1D and 2D; Figs. S2 and S3), as indicated by the bright perimeter surrounding dark pore canals. Density of the material surrounding pore canals was more variable within the endocuticle. Mineralized chitin-protein fibers could be resolved in regions A–D, but were difficult to distinguish in region E due to high overall Z-contrast. When comparing region A in the endocuticle to region D in the denticle, packing density of mineralized fibers tended to be greater in the denticle (Figs. S2–6). The alignment of mineralized chitin-protein fibers also differed between the endocuticle and the denticle. Within the endocuticle, rotating planes of mineralized chitin-protein fibers were visible (i.e. rotating from long axis to short axis of the mineralized chitin-protein fibers within the field of view: Figs. 1–5; Figs. S2–6), consistent with the typical twisted plywood structures of the cuticle [4, 7]. Note that a full rotation of the mineralized chitin-protein fiber planes is not visible in *C. sapidus* due to the wide

spacing of the twisted plywood layers (i.e. as shown in the light microscopy image: Fig. 1). Particularly for *C. sapidus*, *C. borealis*, and *C. opilio*, within the denticle, mineralized chitin-protein fibers are largely aligned parallel to the long axis of the pore canals (Figs. 1–3; Figs. S2–4). For *P. birsteini and P. camtschaticus* a portion of the mineralized chitin-protein fibers align along the long axis of the pore canals whereas others appear at approximately a 45° angle to the long axis of the pore canals.

Another notable difference among species observed by SEM was the structure of the transition zone (i.e., region C). In *C. sapidus, C. opilio, P. birsteini*, and *P. camtschaticus*, the structure of the transition zone closely resembled that of the bulk endocuticle (regions A and B). In contrast, the transition region in *C. borealis* closely resembled the denticle (Fig. 3).

4. Discussion

Crustaceans possess a mineralized exoskeleton that provides resistance to mechanical loads, such as those exerted by predators and during feeding, as well as resistance to changing environmental conditions. In crustaceans, the exoskeleton possesses a great amount of rigidity and strength [2]. The claws of crustaceans are particularly important because they are typically in direct contact with prey items when capturing and opening them. Consequently, it would be beneficial for the claws to have a higher resistance to mechanical loads [24]. Several previous studies have focused on comparing the exoskeleton of the claw to that of the carapace or walking legs [2, 7, 9, 14, 15]. In nearly all cases, mechanical properties of the claw are greatly enhanced, typically showing hardness values 2–3 times that of other body regions [2, 7, 14, 15]. Few studies, however, have compared regions within the claw itself. The goal of this study was to characterize the

mechanical properties of the claw in a range of decapod species, specifically focusing on the denticles, displayed on the inner portions of the dactyl and pollex. We hypothesized that the occurrence of enhanced denticle mechanical properties is widespread among decapod crab species. These structures aid in capturing prey and defense against predators, and to be effective they must show greater reinforcement to prevent wear and damage. Our results support this hypothesis, as a dramatic increase in microhardness from the endocuticle to the denticle was observed in all crab species studied. The magnitude of this difference, however, varied among species, with one species, *P. birsteini*, showing over a ten-fold difference in hardness across the dactylus whereas the change in hardness across the dactylus was less than four-fold in *C. sapidus*.

The decapod cuticle comprises three calcified layers with the exo- and endo cuticle composing the bulk of cuticle thickness. Although the exocuticle in decapod crabs is typically harder than the bulk endocuticle [2, 7], exocuticle hardness is substantially lower (i.e. less than half [7]) than that of the denticles observed here. Observations of the cuticle by light microscopy confirm earlier reports that the denticles are composed of modified endocuticle [16]. In all species, the exocuticle was readily distinguished from the endocuticle within the region of the dactyl proximal to the denticles, and twisted plywood structures (i.e. laminations) that ran along the bulk endocuticle continued through the transition zone into the proximal portion of the denticle. In all species except *P. camtschaticus,* however, the exocuticle ended abruptly as the denticles emerged. This abrupt boundary suggests that the exocuticle fractured and delaminated from the denticle in regions of the denticle surface subjected to sustained wear. For *P. camtschaticus*, the presence of exocuticle may be due to the fact that these crabs were held in captivity for a full

molt cycle before analysis, whereas the other species tested were analyzed directly after collection from the field. During their time in captivity, *P. camtschaticus* were fed a diet of less heavily calcified food items (fish and squid) than they would encounter in the natural environment and were protected from predators. Hence, the denticles in these individuals likely sustained a lower level of wear than they would have experienced in the field.

Structurally, the denticles are reminiscent of the endocuticle "bulge" region of the dorsal carapace in *Cancer pagurus* [6]. These "bulges" of modified endocuticle extend periodically through the outer portion of the cuticle where the exocuticle is typically found; they exhibit enhanced mechanical properties, associated with elevated calcium content. Similar to the denticles, the twisted plywood structures (laminations) run parallel to the carapace surface within the bulk endocuticle but rotate ~90° (normal to the carapace surface) as they approach the "bulge" region. At the periphery of the bulge region, mineralized chitin-protein fibers rotate, but are largely aligned parallel to the long axis of the pore canals, and the diameter of the pore canals is low in this region, again consistent with what was observed in the denticles. Such overall structural arrangement of twisted plywood structure and constituent mineralized chitin-protein fibers may enhance mechanical resistance in the direction normal to the cuticle surface [6, 25, 26]. Although the minerology differs (see below), a shift in structural arrangement of chitin-protein fibers, from twisted plywood structures in the underlying material to alignment of mineral fibers parallel to the long axis of the pore canals within the outer surface, was also shown in mandible teeth of the crayfish *Cherax quadricarinatus* [13].

In four of the five species assessed, the increase in microhardness from the endocuticle to the denticle was significantly correlated with an increase in calcium content (measured as a weight percent using EDS). This result is consistent with previous studies assessing differences in mechanical properties between the walking legs and claw [7] and within regions of the claw [16, 27]. For example, Waugh et al. [16] found elevated hardness of the denticles of *S. serrata* and *C. sapidus*: in both cases denticles were found to be denser, which was presumed to be due to incorporation of greater levels of calcium salts. Qualitative EDS assessments of the claw of *Homarus americanus* also revealed a greater calcium content in regions of the claw found to display higher hardness [27]. Here, although hardness and calcium content were positively correlated in *C. sapidus*, *C. borealis*, *C. opilio,* and *P. camtschaticus*, the magnitude of the increase in calcium content from endocuticle to denticle was far more modest than that of hardness (i.e., a 5–25% increase in calcium vs. 269–1056% increase in hardness). Clearly there is not a one-to-one relationship between calcium content and hardness, suggesting that factors beyond calcium content, for example the nanoscale structure of the mineral, mineralized chitin-protein fiber and fiber plane packing density, or the polymorph of calcium carbonate [2, 6, 12] also influence hardness. In fact, *P. birsteini*, which exhibited the greatest increase in hardness across the cuticle did not show a significant relationship between hardness and calcium content. In this species, calcium content tended to be high throughout the cuticle, implying that enhanced hardness within the denticles is driven largely by the orientation and arrangement of mineralized chitin-protein fibers without a concomitant increase in calcium.

Pore canals are a common feature of the decapod exoskeleton [7, 26, 28]. These structures extend from the hypodermis underlying the cuticle through the endo- and exocuticle, typically

terminating within the proximal portion of the epicuticle [4, 5, 29]. They function in the cuticle formation process, presumably delivering ions to the developing cuticle [4], but also serve an important toughening role [7, 26]. When tested under tension at the macro-scale, the organic tubules within the pore canals show necking behavior, consistent with ductile failure, and may "stich" together mineralized fiber planes [7]. Low-density pores within the otherwise dense mineralized protein-chitin matrix can also deflect incipient cracks [7, 26]. In compression, stress to fracture tends to be greatest when tested normal to the cuticle surface, corresponding to the stiff axis of the pore canals [26]. At the micro-scale, pore canal width was inversely correlated with microhardness in all species, with regions of lower pore canal width (i.e. the denticles) being harder. This trend may result from direct effects of a reduction in the volume fraction occupied by pores in the denticles (i.e. the indentor tip is interacting with a more dense material) and indirect effects of calcium content (i.e. regions of lower pore canal width tended to have higher calcium content). A significant relationship between hardness and pore canal width, however, was still observed in *P. birsteini*, despite the fact that hardness and calcium content were not correlated in this species, suggesting that the relationship between hardness and pore canal width is not solely a byproduct of calcium content. In terms of toughness of the cuticle, it is worth noting that cracks often radiated from indentations in the denticle, but cracks were never observed in the endocuticle. Hence, the dense structural arrangement and low width of pore canals in the denticle may limit deflection of incipient cracks, resulting in a harder, but less tough material.

The decapod cuticle contains both amorphous calcium carbonate (ACC) and nanocrystalline calcite [4, 6, 8, 9]. Regions of the cuticle composed primarily of calcite tend to be harder than

those composed of ACC (at least within the endocuticle "bulge" regions of the carapace: [6]). Both magnesium and phosphate, along with associated proteins, may play a role in the formation and stabilization of amorphous calcium carbonate in biological materials [30, 31]. In all species except *C. sapidus*, magnesium content decreased from endocuticle to denticle, and in all species phosphorus was present in the endocuticle, but completely absent in the denticle. Based on the dramatic difference in hardness between the denticles and endocuticle and the observed trends in magnesium and phosphorus content, one can hypothesize that the denticles are composed exclusively of crystalline calcite while the underlying endocuticle contains a mix of ACC and calcite. Initial FTIR assessments of denticle and non-denticle cuticle support this hypothesis, with denticle consistently showing higher crystallinity than non-denticle cuticle in all species assessed (see Fig. S2 and supporting text).

Crustaceans typically use calcium carbonate to reinforce their exoskeletons, but several orders of crustaceans also use calcium phosphate to reinforce mechanically challenged sites, including feeding structures [11, 32]. Calcium phosphate, often as crystalline fluorapatite, was found in the mandible teeth of species from Astacidea, Dendrobranchiata, Caridea, Isopoda, and Stomatopoda [11]. Interestingly, the presence of calcium phosphate was not universal among crustacean mandibles; the mandible teeth of species from Brachyura and Achelata do not contain phosphorus. The authors suggest that phosphate reinforcement may not be necessary for crustaceans from these groups since they have evolved to embody heavy armor skeletons and overlaying a hard and brittle calcium phosphate layer over calcite may result in a weakened tooth rather than reinforcement [11]. Hence, it may not be surprising that despite the dactylus denticles having similar mechanical needs to mandibular teeth (i.e., resistance to wear and abrasion), EDS

analysis revealed that phosphorus was never identified in the denticles of any of the brachyuran or anomuran species tested here, which precludes the possibility that calcium phosphate is found in the denticles.

Sclerotization, the process of protein and chitin cross-linking within the cuticle, is widely exhibited in Arthropoda as a mechanism of enhancing mechanical resistance of the cuticle [32, 33]. This process, however, is energetically costly and in Crustacea incorporation of minerals may reduce the need for extensive cross-linking [32]. In brachyuran species in which extensive phenolic cross-linking does occur, it is typically restricted to the dactyl and pollex (i.e., the movable and fixed finger) and particularly the contact surface. Of the five species assessed here, *C. borealis* was the only species that displayed a blackened contact surface. This dark coloration is likely the result of phenolic cross-linking of the cuticle [34, 35], although it is important to note that coloration alone cannot confirm the presence of phenolic cross-linking. In *C. borealis,* hardness of the bulk endocuticle tended to be higher than that of the other species assessed, and there was only a modest and gradual increase in hardness at the visual transition to the denticle. If the darkened color of the cuticle in *C. borealis* was indeed due to phenolic cross-linking, enhanced mechanical properties may be due to stiffening imposed by the protein cross-linking itself, or indirectly through reorientation of chitin [34]. Interestingly, if cross-linking was present in *C. borealis*, it did not appear to take the place of mineral incorporation in the claw. Calcium content was actually slightly higher throughout the cuticle in *C. borealis* than in other species. Further, the combination of presumed cross-linking and enhanced mineral content was not additive; although presumed cross-linking and high calcium content co-occurred, hardness of the denticle was no higher than that observed in the other species tested. Given that mounting a hard,

stiff material over a more compliant one may lead to delamination [28], overall structural integrity of the dactyl in *C. borealis* may be enhanced by more closely matching hardness of the denticle to that of the underlying endocuticle.

There were no clear phylogenetic trends apparent in our quantitative data. *P. birsteini* and *P. camtschaticus*, two anomuran species, fell in the middle of the three brachyuran species in the PCA. The species analyzed live in polar, temperate, and tropical climates and in both estuarine and fully marine environments; nevertheless, there was a remarkable degree of similarity among them in their patterns of structural features across the dactylus and mechanical properties of the denticles, supporting our initial hypothesis. This is perhaps not surprising, given that these crabs occupy similar ecological niches and have similar diets, consisting of a large proportion of calcified prey items [e.g., bivalves, gastropods, and crustaceans; 36, 37-40] that require a great deal of mechanical force to consume [41]. These similarities may explain why four out of out five species had very similar maximum hardness in their denticles (220–236 VHN; Table 1). The more resistant the claw, the more force a crab can safely exert without damge to the cuticle. The combination of extrmely high biting force (a product of claw anatomy and muscular properties: [41]) and a highly resitant cuticle would result in greater ease of prey handling and a wider range of food items available for consumption. Claw properties, however, must be balanced against the energetic cost inherent in a larger and stronger claw. Systematic assessment of denticle properties across a diverse range of decapods would be necessary to assess if the similarities in denticle mechanical properties observed here result from common ancestry or if they evolved independently in multiple lineages of decapods (i.e. through convergent evolution).

The one outlier in denticle properties was the blue crab, *C. sapidus,* which separated from all other species in the PCA (see Fig. 6). Although the change in hardness across the cuticle (i.e. from region A to E) was lowest in *C. sapidus,* the maximum hardness in the outer region of the denticles was actually ~20% greater than the other species assessed. Furthermore, magnesium content, which has been shown to enhance hardness when incorporated into biogenic calcite [42, 43], was consistently higher in *C. sapidus* as compared to the other species assessed, and *C. sapidus* was the only species in which a decrease in magnesium content was not observed within the denticle. We hypothesize that elevated denticle hardness in *C. sapidus* could be due to differences in the rate of cannibalism among the species. Although many crab species, including most of the species examined here, are known to exhibit cannibalistic behavior [44-47], *C. sapidus* exhibits an extraordinarily high degree of cannibalism and antagonistic behavior. Cannibalism can account for 75-97% of the mortality of juvenile blue crabs [48], and antagonistic interaction among adults substantially alters foraging patterns [49] and can lead to injury and death [50]. Cannibalism in *C. sapidus* is strongly size-dependent [e.g., 51], and they are much less likely to attack a conspecific that has a claw strength capable of injuring the attacker [52]. Thus, the rate of cannibalism in blue crabs may provide an evolutionary advantage to crabs with more mechanically robust claws.

5. Conclusions

Claw wear and breakage can reduce the efficiency with which crabs capture prey [18], and may also inhibit their ability to fight and reproduce. Hence, an increase in hardness of the claw, specifically in the denticles which typically withstand the greatest amount of mechanical stress, is essential for maintaining a crab's fitness [17, 18, 53]. This strong evolutionary pressure has

likely driven development of the robust denticles observed in the brachyuran and anomuran species tested here. Although enhanced denticle hardness was observed in all species tested, the mechanisms underlying these trends, particularly with respect to mineral content, vary from species to species. Further characterization of the mechanical properties, elemental composition, and macro- and microstructure across a wide variety of decapods will heighten our understanding of decapod evolution, allow us to identify cuticular alterations that result from environmental change (e.g., ocean acidification: [14]), and enable application of the strategies employed by these organisms to creating novel materials.

Acknowledgments

This project was partially funded by the National Oceanic and Atmospheric Administration (NOAA) Ocean Acidification Program (W.C.L & R.J.F.) and the U.S. National Science Foundation (grant ANT-1141877 to R.B.A.). K.A.B. and J.N.S. were supported by The College of New Jersey's Mentored Undergraduate Research Experience (MUSE). The findings and conclusions in the paper are those of the authors and do not necessarily represent the views of the National Marine Fisheries Service, NOAA. Reference to trade names does not imply endorsement by the National Marine Fisheries Service, NOAA. This is contribution no. 225 from the Institute for Global Ecology at the Florida Institute of Technology.

References

[1] M.A. Meyers, A.Y. Lin, Y. Seki, P.-Y. Chen, B.K. Kad, S. Bodde, Structural biological composites: an overview, J.O.M. 58 (2006) 35-41.

[2] J. Lian, J. Wang, Microstructure and mechanical properties of dungeness crab exoskeletons, in: T. Proulx (Ed.), Mechanics of Biological Systems and Materials, Volume 2, Springer, New York, 2011, pp. 93-99.

[3] J.C. Weaver, G.W. Milliron, A. Miserez, K. Evans-Lutterodt, S. Herrera, I. Gallana, W.J. Mershon, B. Swanson, P. Zavattieri, E. DiMasi, The stomatopod dactyl club: a formidable damage-tolerant biological hammer, Science 336 (2012) 1275-1280.

[4] R. Roer, R. Dillaman, The structure and calcification of the crustacean cuticle, Am. Zool. 24 (1984) 893-909.

[5] T. Hegdahl, F. Gustavsen, J. Silness, The structure and mineralization of the carapace of the crab (*Cancer pagurus* L.) 3. The epicuticle, Zool. Scr. 6 (1977) 215-220.

[6] H.-O. Fabritius, E.S. Karsten, K. Balasundaram, S. Hild, K. Huemer, D. Raabe, Correlation of structure, composition and local mechanical properties in the dorsal carapace of the edible crab *Cancer pagurus*, Z. Kristallogr. Cryst. Mater. 227 (2012) 766-776.

[7] P.-Y. Chen, A.Y.-M. Lin, J. McKittrick, M.A. Meyers, Structure and mechanical properties of crab exoskeletons, Acta Biomater. 4 (2008) 587-596.

[8] R. Dillaman, S. Hequembourg, M. Gay, Early pattern of calcification in the dorsal carapace of the blue crab, *Callinectes sapidus*, J. Morphol. 263 (2005) 356-374.

[9] F. Boßelmann, P. Romano, H. Fabritius, D. Raabe, M. Epple, The composition of the exoskeleton of two crustacea: The American lobster *Homarus americanus* and the edible crab *Cancer pagurus*, Thermochim. Acta 463 (2007) 65-68.

[10] C. Sachs, H. Fabritius, D. R-Aabe, Influence of microstructure on deformation anisotropy of mineralized cuticle from the lobster *Homarus americanus*, J. Struct. Biol. 161 (2008) 120-132.

[11] S. Bentov, E.D. Aflalo, J. Tynyakov, L. Glazer, A. Sagi, Calcium phosphate mineralization is widely applied in crustacean mandibles, Sci. Rep. 6 (2016) 22118.

[12] H.-O. Fabritius, A. Ziegler, M. Friák, S. Nikolov, J. Huber, B.H. Seidl, S. Ruangchai, F.I. Alagboso, S. Karsten, J. Lu, Functional adaptation of crustacean exoskeletal elements through structural and compositional diversity: a combined experimental and theoretical study, Bioinspiration Biomim. 11 (2016) 055006.

[13] S. Bentov, P. Zaslansky, A. Al-Sawalmih, A. Masic, P. Fratzl, A. Sagi, A. Berman, B. Aichmayer, Enamel-like apatite crown covering amorphous mineral in a crayfish mandible, Nat. Commun. 3 (2012) 839.

[14] W.D. Coffey, J.A. Nardone, A. Yarram, W.C. Long, K.M. Swiney, R.J. Foy, G.H. Dickinson, Ocean acidification leads to altered micromechanical properties of the mineralized cuticle in juvenile red and blue king crabs, J. Exp. Mar. Biol. Ecol. 495 (2017) 1-12.

[15] B.V. Steffel, K.E. Smith, G.H. Dickinson, J.A. Flannery, K.A. Baran, M.N. Rosen, J.B. McClintock, R.B. Aronson, Characterization of the exoskeleton of the Antarctic king crab *Paralomis birsteini*, Invertebr. Biol. (2019) e12246.

[16] D.A. Waugh, R.M. Feldmann, A.M. Schroeder, M.H. Mutel, Differential cuticle architecture and its preservation in fossil and extant *Callinectes* and *Scylla* claws, J. Crustacean Biol. 26 (2006) 271-282.

[17] R.M. Schofield, J.C. Niedbala, M.H. Nesson, Y. Tao, J.E. Shokes, R.A. Scott, M.J. Latimer, Br-rich tips of calcified crab claws are less hard but more fracture resistant: A comparison of mineralized and heavy-element biological materials, J. Struct. Biol. 166 (2009) 272-287.

[18] F. Juanes, E. Hartwick, Prey size selection in Dungeness crabs: the effect of claw damage, Ecology 71 (1990) 744-758.

[19] C. Noever, H. Glenner, The origin of king crabs: hermit crab ancestry under the magnifying glass, Zool. J. Linnean Soc. 182 (2017) 300-318.

[20] S. Hall, S. Thatje, Evolution through cold and deep waters: the molecular phylogeny of the Lithodidae (Crustacea: Decapoda), Sci. Nat. 105 (2018) 19.

[21] K.E. Smith, R.B. Aronson, B.V. Steffel, M.O. Amsler, S. Thatje, H. Singh, J. Anderson, C.J. Brothers, A. Brown, D.S. Ellis, Climate change and the threat of novel marine predators in Antarctica, Ecosphere 8 (2017) e02017.

[22] C. Lang, J. Richar, R.J. Foy, The 2017 eastern Bering Sea continental shelf and northern Bering Sea bottom trawl surveys: results for commercial crab species. NOAA Technical Memorandum NMFS-AFSC-372, U.S. Department of Commerce, Kodiak, AK, 2018.

[23] C.A. Schneider, W.S. Rasband, K.W. Eliceiri, NIH Image to ImageJ: 25 years of image analysis, Nat. Methods 9 (2012) 671-675.

[24] F. Zhou, Z. Wu, M. Wang, K. Chen, Structure and mechanical properties of pincers of lobster (*Procambarus clarkii*) and crab (*Eriocheir Sinensis*), J. Mech. Behav. Biomed. Mater. 3 (2010) 454-463.

[25] S. Nikolov, H. Fabritius, M. Petrov, M. Friák, L. Lymperakis, C. Sachs, D. Raabe, J. Neugebauer, Robustness and optimal use of design principles of arthropod exoskeletons studied by ab initio-based multiscale simulations, J. Mech. Behav. Biomed. Mater. 4 (2011) 129-145.

[26] H. Fabritius, C. Sachs, D. Raabe, S. Nikolov, M. Friák, J. Neugebauer, Chitin in the exoskeletons of arthropoda: from ancient design to novel materials science, in: N.S. Gupta (Ed.), Chitin: formation and diagenesis, Dordrecht, 2011, pp. 35-60.

[27] C. Sachs, H. Fabritius, D. Raabe, Hardness and elastic properties of dehydrated cuticle from the lobster *Homarus americanus* obtained by nanoindentation, J. Mater. Res. 21 (2006) 1987-1995.

[28] D.F. Travis, Structural features of mineralization from tissue to macromolecular levels of organization in the decapod Crustacea, Ann. N.Y. Acad. Sci. 109 (1963) 177-245.

[29] L. Addadi, S. Raz, S. Weiner, Taking advantage of disorder: amorphous calcium carbonate and its roles in biomineralization, Adv. Mater. 15 (2003) 959-970.

[30] S. Weiner, Y. Levi-Kalisman, S. Raz, L. Addadi, Biologically formed amorphous calcium carbonate, Connect Tissue Res. 44 (2003) 214-218.

[31] S. Bentov, S. Abehsera, A. Sagi, The mineralized exoskeletons of crustaceans, in: E. Cohen, B. Moussain (Eds.), Extracellular Composite Matrices in Arthropods, Springer, 2016, pp. 137-163.

[32] Y. Politi, B. Bar-On, H.-O. Fabritius, Mechanics of arthropod cuticle-versatility by structural and compositional variation, in: Y. Estrin, Y. Brechet, J. Dunlop, P. Fratzl (Eds), Architectured Materials in Nature and Engineering, Springer, 2019, pp. 287-327.

[33] C. Melnick, Z. Chen, J. Mecholsky, Hardness and toughness of exoskeleton material in the stone crab, *Menippe mercenaria*, J. Mater. Res. 11 (1996) 2903-2907.

[34] G. Krishnan, Phenolic tanning and pigmentation of the cuticle in *Carcinus maenas*, J. Cell Sci. 3 (1951) 333-342.

[35] M.A. Meyers, P.-Y. Chen, Biological Materials Science: Biological Materials, Bioinspired Materials, and Biomaterials, Cambridge University Press, Cambridge, 2014.

[36] S. Jewett, H. Feder, Food and feeding habits of the king crab *Paralithodes camtschatica* near Kodiak Island, Alaska, Mar. Biol. 66 (1982) 243-250.

[37] R.A. Laughlin, Feeding habits of the blue crab, *Callinectes sapidus* Rathbun, in the Apalachicola estuary, Florida, Bull. Mar. Sci. 32 (1982) 807-822.

[38] K.E. Smith, R.B. Aronson, S. Thatje, G.A. Lovrich, M.O. Amsler, B.V. Steffel, J.B. McClintock, Biology of the king crab *Paralomis birsteini* on the continental slope off the western Antarctic Peninsula, Polar Biol. 40 (2017) 2313-2322.

[39] L.L. Stehlik, Diets of the brachyuran crabs *Cancer irroratus*, *C. borealis*, and *Ovalipes ocellatus* in the New York Bight, J. Crustacean Biol. 13 (1993) 723-735.

[40] M. Tarverdieva, On Feeding of Snow Crabs *Chionoecetes opilio* and *Ch. bairdi* in the Bering Sea, Zool. Zh. 60 (1981) 991-998.

[41] G.M. Taylor, Maximum force production: why are crabs so strong?, Proc. R. Soc. Lond. B 267 (2000) 1475-1480.

[42] M.E. Kunitake, L.M. Mangano, J.M. Peloquin, S.P. Baker, L.A. Estroff, Evaluation of strengthening mechanisms in calcite single crystals from mollusk shells, Acta Biomater. 9 (2013) 5353-5359.

[43] M.E. Kunitake, S.P. Baker, L.A. Estroff, The effect of magnesium substitution on the hardness of synthetic and biogenic calcite, MRS Commun. 2 (2012) 113-116.

[44] A.H. Hines, A.M. Haddon, L.A. Wiechert, Guild structure and foraging impact of blue crabs and epibenthic fish in a subestuary of Chesapeake Bay, Mar. Ecol. Prog. Ser. 6 (1990) 105-126.

[45] W.C. Long, E.F. Gamelin, E.G. Johnson, A.H. Hines, Density-dependent indirect effects: apparent mutualism and apparent competition coexist in a two-prey system, Mar. Ecol. Prog. Ser. 456 (2012) 139-148.

[46] W.C. Long, L. Whitefleet-Smith, Cannibalism in red king crab: Habitat, ontogeny, and the predator functional response, J. Exp. Mar. Biol. Ecol. 449 (2013) 142-148.

[47] G.A. Lovrich, B. Sainte-Marie, Cannibalism in the snow crab, *Chionoecetes opilio* (O. Fabricius)(Brachyura: Majidae), and its potential importance to recruitment, J. Exp. Mar. Biol. Ecol. 211 (1997) 225-245.

[48] A.H. Hines, G.M. Ruiz, Temporal variation in juvenile blue crab mortality: nearshore shallows and cannibalism in Chesapeake Bay, Bull. Mar. Sci. 57 (1995) 884-901.

[49] A.H. Hines, W.C. Long, J.R. Terwin, S.F. Thrush, Facilitation, interference, and scale: the spatial distribution of prey patches affects predation rates in an estuarine benthic community, Mar. Ecol. Prog. Ser. 385 (2009) 127-135.

[50] R.A. Mansour, R.N. Lipcius, Density-dependent foraging and mutual interference in blue crabs preying upon infaunal clams, Mar. Ecol. Prog. Ser. 72 (1991) 239.

[51] J.-D. Dutil, J. Munro, M. Peloquin, Laboratory study of the influence of prey size on vulnerability to cannibalism in snow crab (*Chionoecetes opilio* O. Fabricius, 1780), J. Exp. Mar. Biol. Ecol. 212 (1997) 81-94.

[52] J. Dutil, C. Rollet, R. Bouchard, W. Claxton, Shell strength and carapace size in non-adult and adult male snow crab (Chionoecetes opilio), J. Crustacean Biol. 20 (2000) 399-406.

[53] S.C. Brown, S.R. Cassuto, R.W. Loos, Biomechanics of chelipeds in some decapod crustaceans, J. Zool. 188 (1979) 143-159.

Figure legends

Figure 1. *Callinectes sapidus.* Middle panel: light microscopy image of a dactylus cross section. Top row displays SEM images taken at 5000 X for each of the five regions (A–E) marked on the light microscopy image. Region C corresponds to the transition between endocuticle and denticle. The cuticle is composed of mineralized chitin-protein fibers, "CF", several of which are bracketed in image A, and surround pore canals, "PC." Scale bar for SEM images is 4 μm. Bottom: Microhardness testing along a transect running across the section. Measurements taken within the denticle are shown in the shaded box. Indents are visible as a row of diamonds in the light microscopy image, and each plotted hardness data point is aligned with its respective indent in the image.

Figure 2. *Cancer borealis.* Middle panel: light microscopy image of a dactylus cross section. Top row displays SEM images taken at 5000 X for each of the five regions (A–E) marked on the light microscopy image. Region C corresponds to the transition between endocuticle and denticle. The cuticle is composed of mineralized chitin-protein fibers, "CF", several of which are bracketed in image A, and surround pore canals, "PC." Scale bar for SEM images is 4 μm. Bottom: Microhardness testing along a transect running across the section. Measurements taken within the denticle are shown in the shaded box. Indents are visible as a row of diamonds in the light microscopy image, and each plotted hardness data point is aligned with its respective indent in the image.

Figure 3. *Chionoecetes opilio.* Middle panel: light microscopy image of a dactylus cross section. Top row displays SEM images taken at 5000 X for each of the five regions (A–E) marked on the light microscopy image. Region C corresponds to the transition between endocuticle and denticle. The cuticle is composed of mineralized chitin-protein fibers, "CF", several of which are bracketed in image A, and surround pore canals, "PC." Scale bar for SEM images is 4 μm. Bottom: Microhardness testing along a transect running across the section. Measurements taken within the denticle are shown in the shaded box. Indents are visible as a row of diamonds in the light microscopy image, and each plotted hardness data point is aligned with its respective indent in the image.

Figure 4. *Paralomis birsteini.* Middle panel: light microscopy image of a dactylus cross section. Top row displays SEM images taken at 5000 X for each of the five regions (A–E) marked on the light microscopy image. Region C corresponds to the transition between endocuticle and denticle. The cuticle is composed of mineralized chitin-protein fibers, "CF", several of which are bracketed in image A, and surround pore canals, "PC." Scale bar for SEM images is 4 μm.

Bottom: Microhardness testing along a transect running across the section. Measurements taken within the denticle are shown in the shaded box. Indents are visible as a row of diamonds in the light microscopy image, and each plotted hardness data point is aligned with its respective indent in the image.

Figure 5. *Paralithodes camtschaticus.* Middle panel: light microscopy image of a dactylus cross section. Top row displays SEM images taken at 5000 X for each of the five regions (A–E) marked on the light microscopy image. Region C corresponds to the transition between endocuticle and denticle. The cuticle is composed of mineralized chitin-protein fibers, "CF", several of which are bracketed in image A, and surround pore canals, "PC." Scale bar for SEM images is 4 μm. Bottom: Microhardness testing along a transect running across the section. Measurements taken within the denticle are shown in the shaded box. Indents are visible as a row of diamonds in the light microscopy image, and each plotted hardness data point is aligned with its respective indent in the image. As shown in the middle panel, a small amount of exocuticle ("exo") was visible in *P. camtschaticus*.

Figure 6: Principal component plot of observations of crab dactylus cuticle properties (microhardness, elemental content, and structure) in five crab species. Data were normalized prior to analysis (see text for details). Point labels represent areas A–E of the cuticle (see text for description). Vectors indicate the loading of each of the variables.

Table 1. Summary statistics for elemental and microhardness data (mean ± standard deviation). Locations of regions A–E are shown in Figs. 1–5. Sample sizes: n = 3 replicate dactyli per species except in *Paralithodes camtschaticus*, for which n = 2 replicate dactyli.

	Endocuticle		**Transition**	**Denticle**		**% Change from A to E**
	A	**B**	**C**	**D**	**E**	
Callinectes sapidus						
Microhardness (VHN)	75.2 ± 12.9	54.4 ± 11.1	82.3 ± 69.0	198.1 ± 0.7	271.8 ± 4.7	+ 269 ± 64
Ca (wt %)	29.5 ± 4.1	34.4 ± 0.4	33.7 ± 2.3	35.7 ± 0.4	36.1 ± 1.1	+ 25 ± 23
Mg (wt %)	1.5 ± 0.2	1.9 ± 0.2	1.9 ± 0.2	1.9 ± 0.2	1.7 ± 0.2	+ 11 ± 8
P (wt %)	0.9 ± 0.1	1.0 ± 0.1	0.5 ± 0.4	0 ± 0	0 ± 0	– 100 ± 0
Pore canal width	0.41 ± 0.08	0.47 ± 0.12	0.54 ± 0.15	0.33 ± 0.10	0.23 ± 0.06	- 41 ± 26
Cancer borealis						
Microhardness (VHN)	59 ± 26	137 ± 51	184 ± 14	222 ± 4	220 ± 13	+ 311 ± 140
Ca (wt %)	35.5 ± 0.7	37.1 ± 0.6	38.3 ± 0.5	38.6 ± 0.7	38.0 ± 0.4	+ 7 ± 3
Mg (wt %)	1.25 ± 0.12	1.12 ± 0.04	0.81 ± 0.12	0.69 ± 0.15	0.53 ± 0.08	– 57 ± 6
P (wt %)	0.28 ± 0.29	0.04 ± 0.04	0 ± 0	0 ± 0	0 ± 0	– 100 ± 0
Pore canal width	1.09 ± 0.24	1.14 ± 0.26	0.70 ± 0.19	0.39 ± 0.03	0.27 ± 0.04	– 74 ± 8
Chionoecetes opilio						
Microhardness (VHN)	43 ± 6	65 ± 29	66 ± 2	204 ± 52	236 ± 9	+ 459 ± 84
Ca (wt %)	29.4 ± 2.2	32.0 ± 1.8	33.7 ± 0.3	37.3 ± 0.8	36.9 ± 0.9	+ 26 ± 12
Mg (wt %)	0.86 ± 0.15	0.78 ± 0.42	0.64 ± 0.28	0.42 ± 0.10	0.27 ± 0.06	– 68 ± 9
P (wt %)	0.28 ± 0.07	0.29 ± 0.05	0.20 ± 0.07	0 ± 0	0 ± 0	–100 ± 0
Pore canal width	0.67 ± 0.19	0.76 ± 0.32	0.87 ± 0.24	0.35 ± 0.04	0.25 ± 0.02	– 59 ± 17
Paralomis birsteini						
Microhardness (VHN)	23 ± 12	53 ± 9	98 ± 18	227 ± 9	224 ± 5	+ 1056 ± 504
Ca (wt %)	35.5 ± 2.2	37.2 ± 0.4	37.9 ± 0.4	37.8 ± 0.1	37.1 ± 1.2	+ 5 ± 3
Mg (wt %)	1.4 ± 0.2	1.4 ± 0.2	1.3 ± 0.2	1.4 ± 0.3	1.0 ± 0.1	– 28 ± 5
P (wt %)	0.62 ± 0.20	0.26 ± 0.01	0.07 ± 0.12	0 ± 0	0 ± 0	– 100 ± 0
Pore canal width	0.79 ± 0.11	0.82 ± 0.08	0.78 ± 0.10	0.56 ± 0.09	0.33 ± 0.08	– 68 ± 11
Paralithodes camtschaticus						
Microhardness (VHN)	44 ± 4	51 ± 2	123 ± 28	232 ± 1	226 ± 12	+ 422 ± 19
Ca (wt %)	34.03 ± 0.00	35.31 ± 0.14	36.39 ± 0.55	37.69 ± 0.18	37.52 ± 0.19	+ 10 ± 1
Mg (wt %)	1.22 ± 0.28	1.22 ± 0.15	1.18 ± 0.11	1.07 ± 0.09	1.06 ± 0.06	– 12 ± 15
P (wt %)	0.46 ± 0.10	0.48 ± 0.13	0.41 ± 0.05	0 ± 0	0 ± 0	– 100 ± 0
Pore canal width	0.79 ± 0.02	0.74 ± 0.05	0.57 ± 0.07	0.24 ± 0.10	0.29 ± 0.09	– 63 ± 10

Table 2: Principal component analysis of crab cuticle hardness, elemental composition, and pore canal width.

	Eigenvalues	**% Variation**	**Cum. % Variation**
PC1	2.6	51.0	51.0
PC2	1.1	21.6	72.6
PC3	0.8	15.7	88.3
	Eigenvectors		
Variable	**PC1**	**PC2**	**PC3**
Ca (wt %)	0.444	-0.073	0.632
Mg (wt %)	-0.311	0.586	0.634
P (wt %)	-0.524	0.306	-0.084
Microhardness	0.569	0.253	0.028
Pore canal width	-0.329	-0.702	0.437

Table 3. Spearman rank correlation analyses. Statistical significance was determined using a Benjamini-Hochberg procedure at a false discovery rate of 0.1. Bold values indicate significant relationships.

	Spearman's ρ	**p-value**
Callinectes sapidus		
Ca vs. Microhardness	**0.568**	**0.027**
Mg vs. Microhardness	-0.096	0.545
Pore canal width vs. Microhardness	**-0.675**	**0.006**
Cancer borealis		
Ca vs. Microhardness	**0.700**	**0.004**
Mg vs. Microhardness	**-0.882**	**0.000**
Pore canal width vs. Microhardness	**-0.775**	**0.001**
Chionoecetes opilio		
Ca vs. Microhardness	**0.696**	**0.004**
Mg vs. Microhardness	**-0.714**	**0.003**
Pore canal width vs. Microhardness	**-0.621**	**0.013**
Paralomis birsteini		
Ca vs. Microhardness	0.371	0.173
Mg vs. Microhardness	-0.156	0.580
Pore canal width vs. Microhardness	**-0.743**	**0.002**
Paralithodes camtschaticus		
Ca vs. Microhardness	**0.875**	**0.001**
Mg vs. Microhardness	-0.570	0.085
Pore canal width vs. Microhardness	**-0.879**	**0.001**

Figure 1

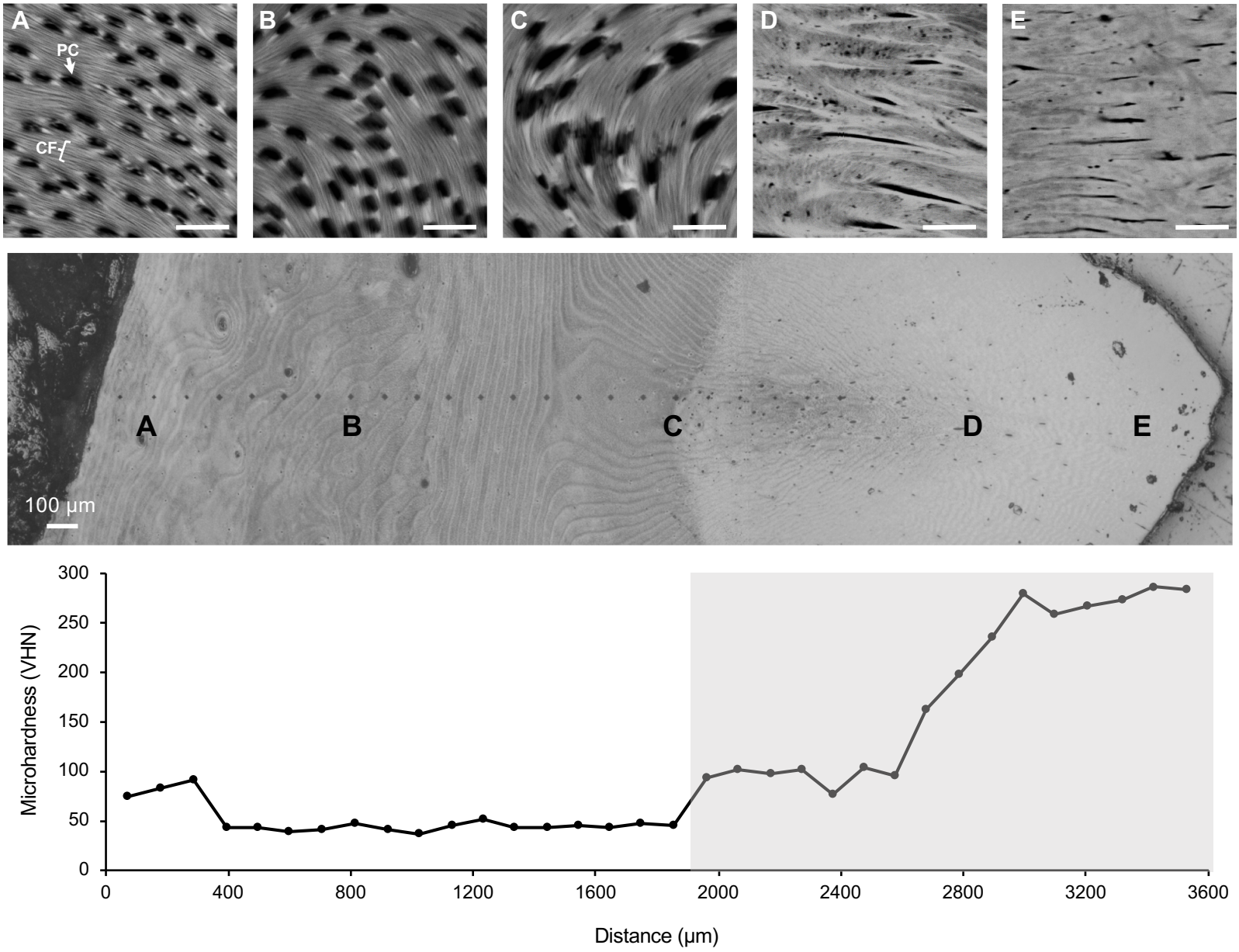
A
PC
CF
B
C
D
E
A
B
C
D
E
100 µm
Microhardness (VHN)
300
250
200
150
100
50
0
0
400
800
1200
1600
2000
2400
2800
3200
3600
Distance (µm)

Figure 2

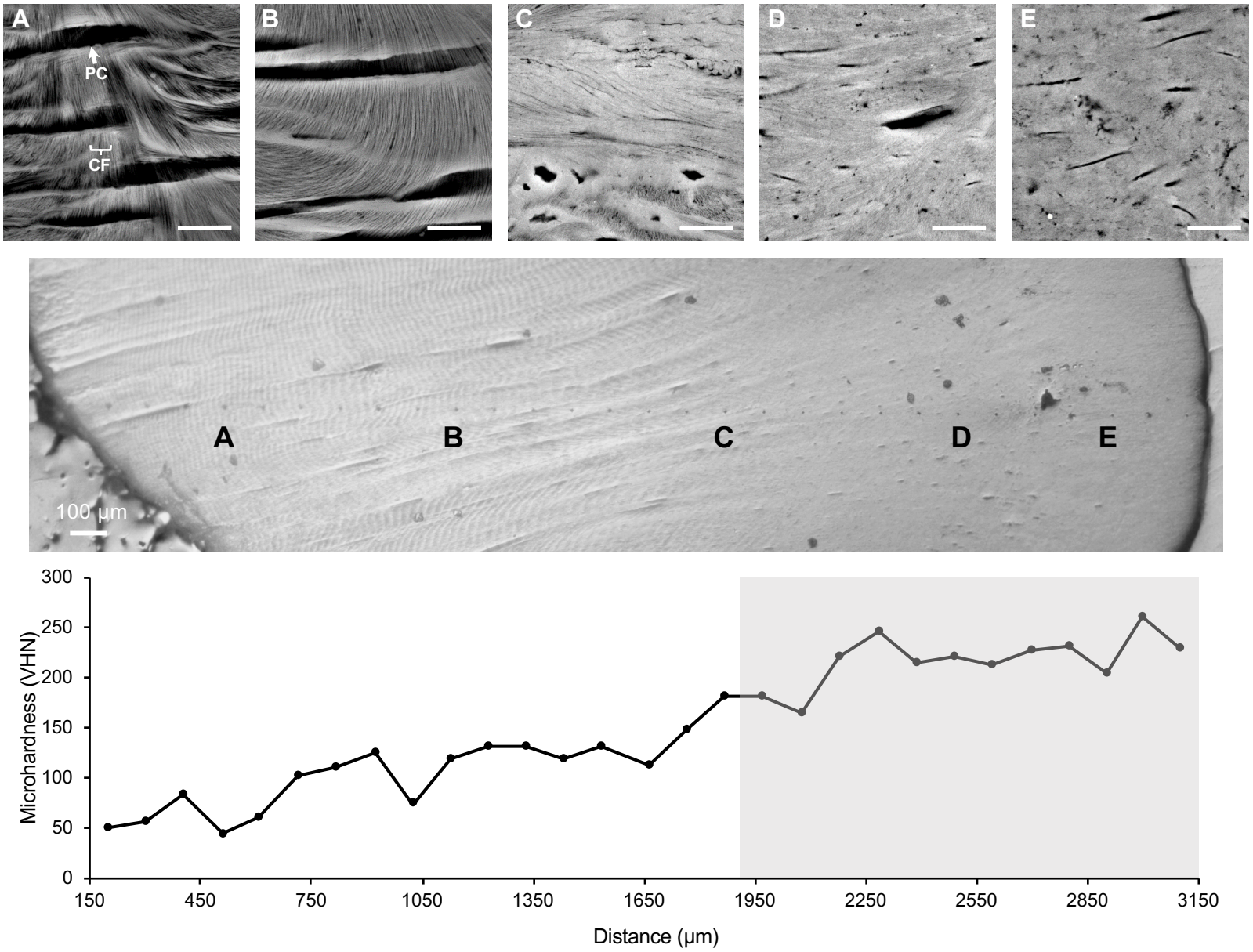
A
PC
CF
B
C
D
E
A
B
C
D
E
100 µm
Microhardness (VHN)
300
250
200
150
100
50
0
150
450
750
1050
1350
1650
1950
2250
2550
2850
3150
Distance (µm)

Figure 3

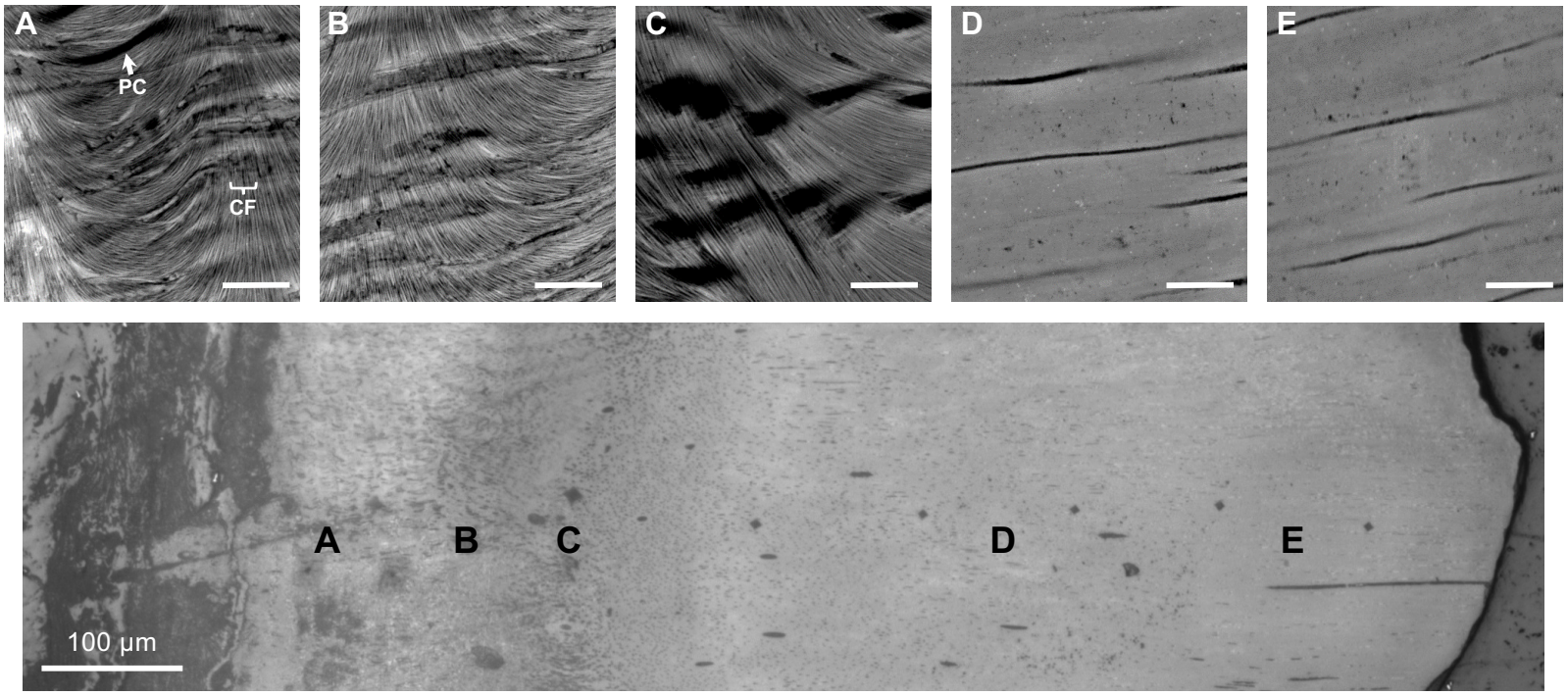
A
PC
CF
B
C
D
E
A
B
C
D
E
100 µm

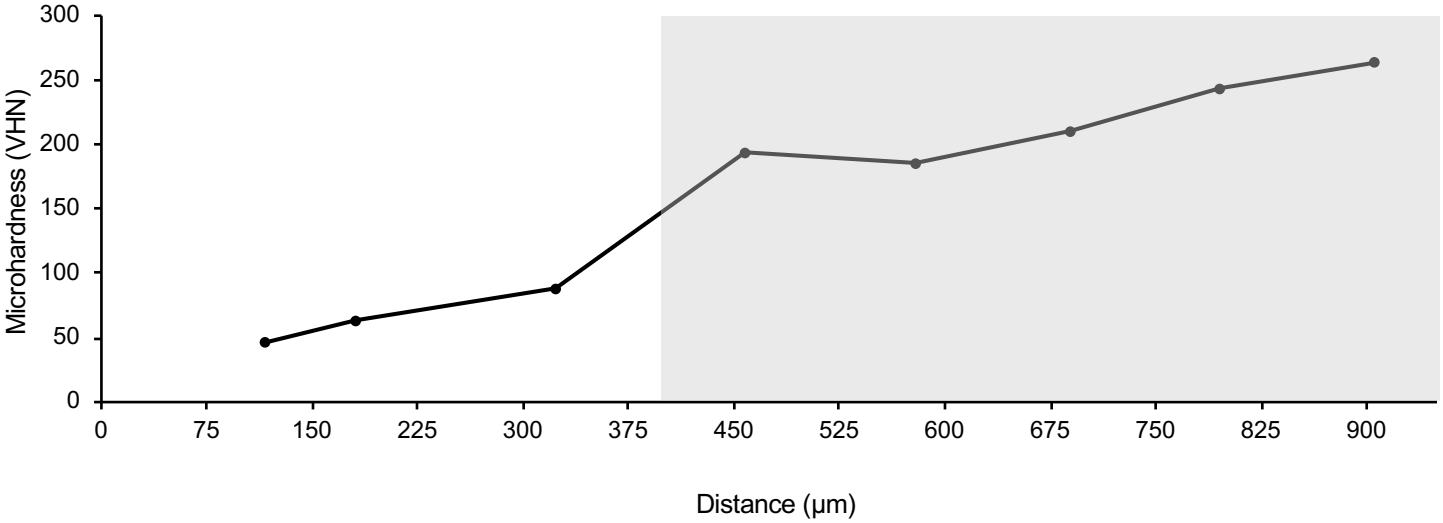
Microhardness (VHN)
300
250
200
150
100
50
0
0
75
150
225
300
375
450
525
600
675
750
825
900
Distance (µm)

Figure 4

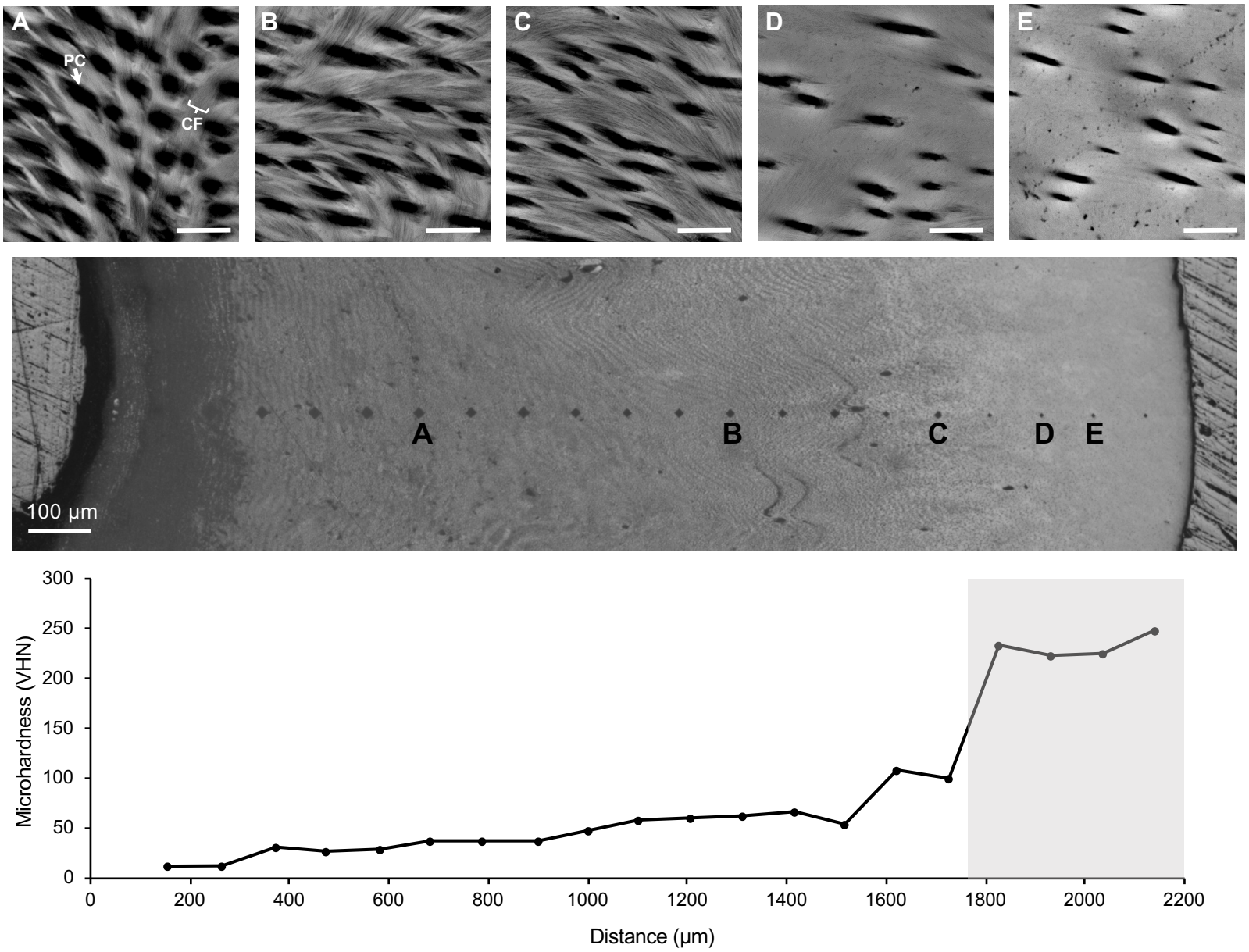
A
PC
CF
B
C
D
E
A
B
C
D
E
100 µm
Microhardness (VHN)
300
250
200
150
100
50
0
0
200
400
600
800
1000
1200
1400
1600
1800
2000
2200
Distance (µm)

Figure 5

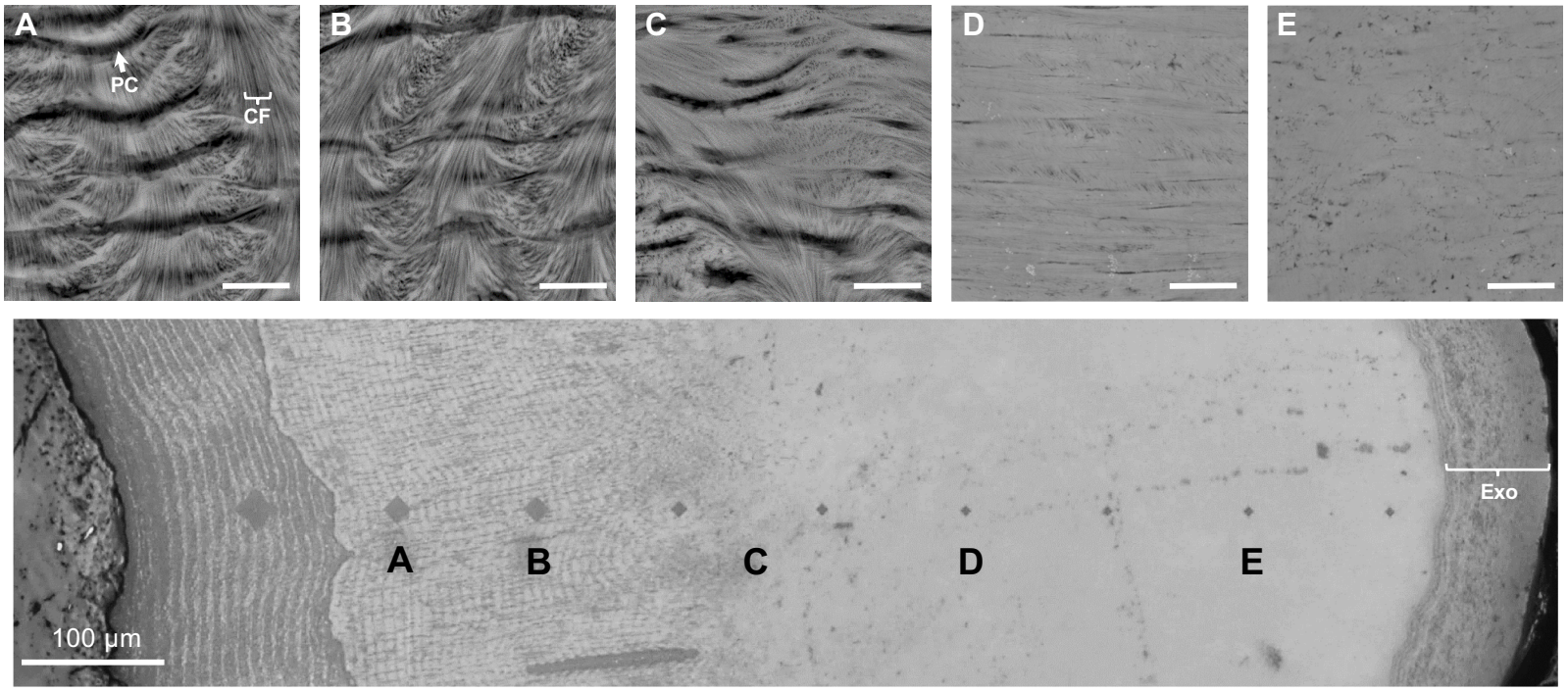
A
PC
CF
B
C
D
E
A
B
C
D
E
Exo
100 µm

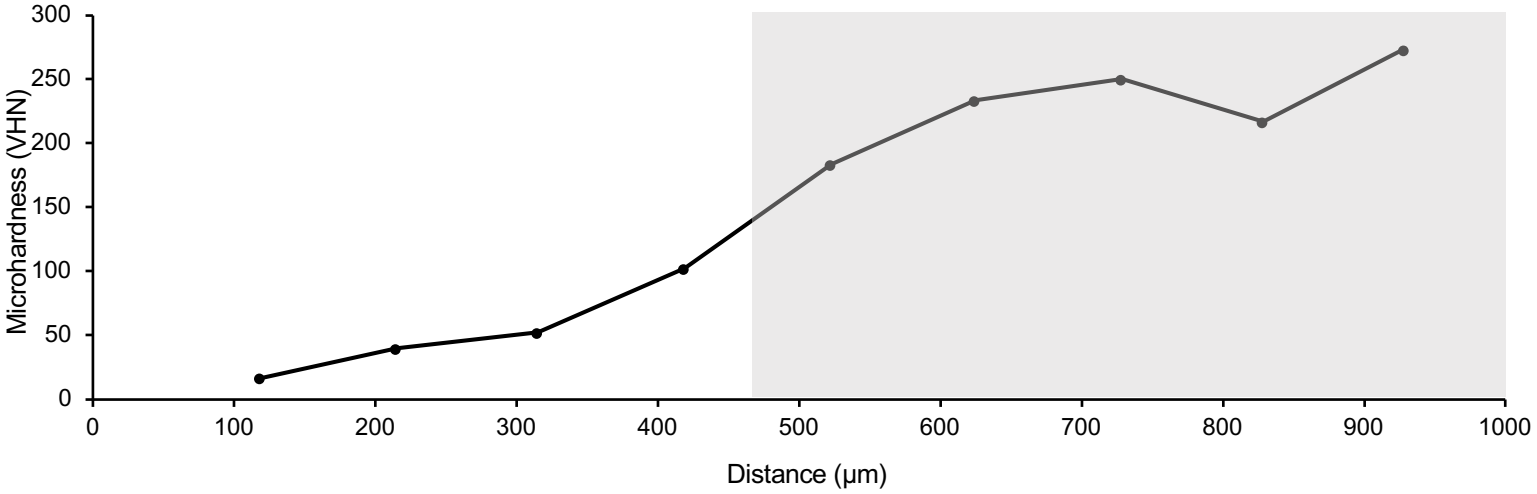
Microhardness (VHN)
300
250
200
150
100
50
0
0
100
200
300
400
500
600
700
800
900
1000
Distance (µm)

Figure 6

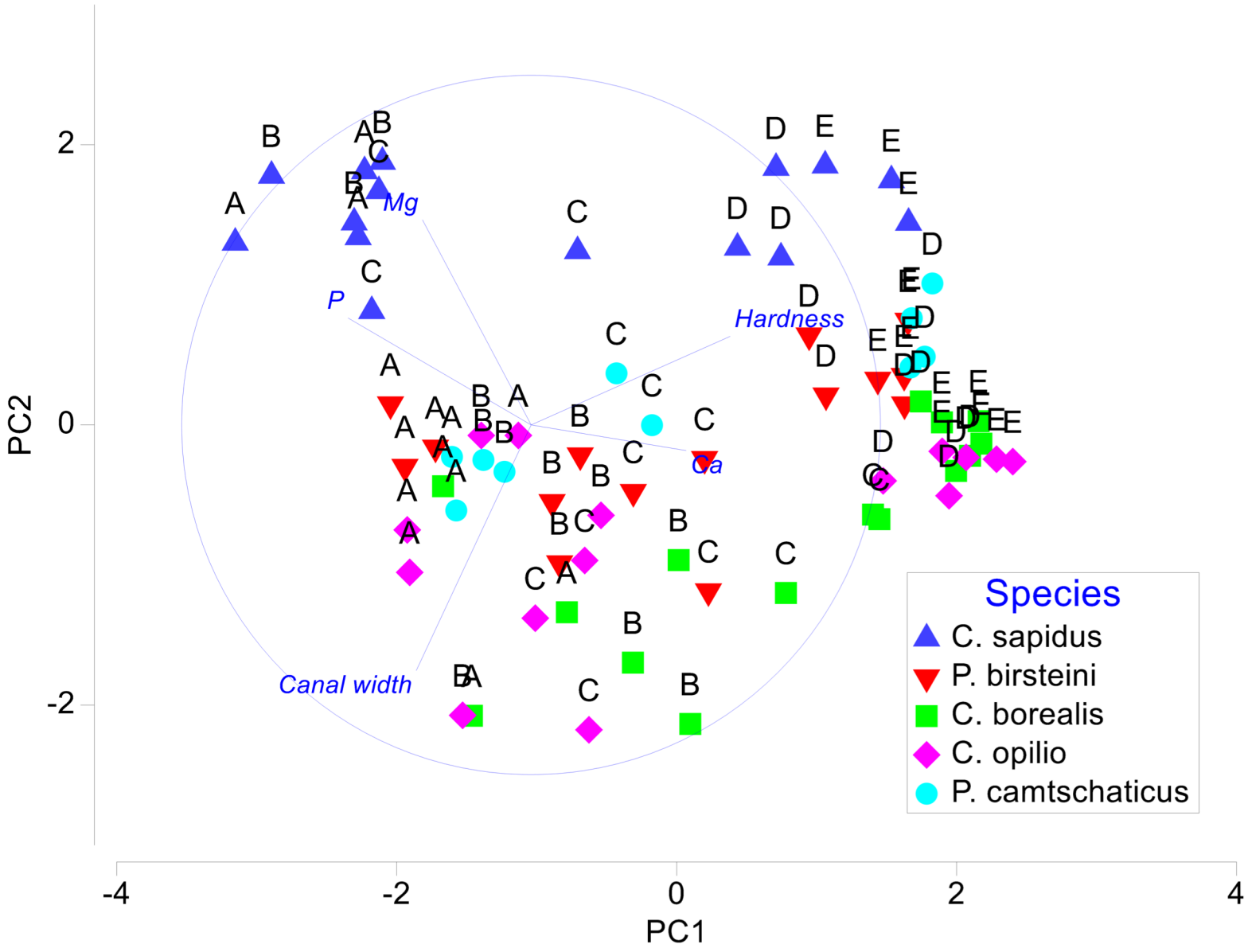
PC2
PC1
2
0
-2
-4
-2
0
2
4
Mg
P
Hardness
Ca
Canal width
Species
C. sapidus
P. birsteini
C. borealis
C. opilio
P. camtschaticus

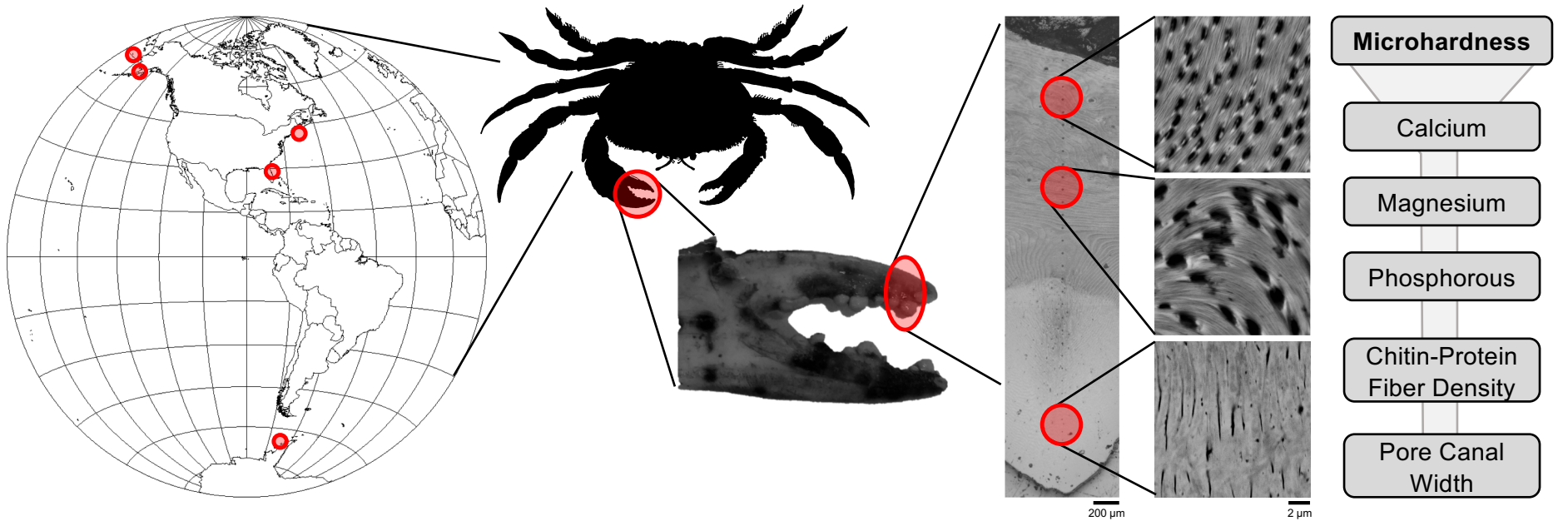
Microhardness
Calcium
Magnesium
Phosphorous
Chitin-Protein Fiber Density
Pore Canal Width
200 µm
2 µm